Journal of Marine Science and Application (2025) 24: 1037-1048
https://doi.org/10.1007/s11804-025-00671-y

RESEARCH ARTICLE

Method of Bionic Fish Scale Structure on Pressure Fluctuation Suppression of a Centrifugal Pump

Xingyu Jia[1], Qixuan Sun[1], Xuechu Zhao[2], Bing Liu[3] and Lei Tan[1]

Received: 19 September 2024 / Accepted: 11 October 2024

Abstract

Centrifugal pumps are extensively employed in ocean engineering, such as ship power systems, water transportation, and mineral exploitation. Pressure fluctuation suppression is essential for the operation stability and service life of the centrifugal pump. In this paper, a new method of bionic structure is proposed for the blade surface of a centrifugal pump, which is inspired by the fish scale and comprises a leading edge, a trailing edge, and two symmetrical side edges. This fish scale structure is applied to the blade pressure and suction surfaces, and an impeller with a fish scale structure is constructed. A test rig for a centrifugal pump is developed to determine the pressure fluctuation in the pump with a prototype impeller and fish scale structure impeller. Results reveal that the dominant frequency of pressure fluctuation in volute is the blade passing frequency (f_{bpf}) of 193.33 Hz, which is triggered by the interaction between the tongue and the impeller. The bionic structure of the fish scale effectively suppresses the pressure fluctuation amplitude at f_{bpf}. From flow rates of 0.6 Q_d to 1.2 Q_d, the average suppressions in pressure fluctuation amplitudes at f_{bpf} are 20.98%, 5.85%, 19.20%, and 25.77%.

Keywords Pressure fluctuation; Centrifugal pump; Fish scale; Bionic structure; Blade passing frequency

1 Introduction

Energy conversion and fluid transportation are substantially influenced by pumps, which are extensively employed in various engineering applications, including petrochemical engineering, water conservation projects, aerospace, and ocean engineering (Yin et al., 2020; Fu et al., 2016; Lu and Tan, 2024; Duplaa et al., 2010). The world is presently facing urgent energy challenges and rising environmental problems. Industries have established stricter standards and expectations for the efficiency, reliability, and acoustic performance of centrifugal pumps (Van and Pretorius, 2018).

Pressure fluctuation during operation is triggered by the interaction between the tongue and impeller (Majidi, 2005). These fluctuations are directly linked to vibrations. Hence, studying the properties of pressure fluctuations within centrifugal pumps holds remarkable importance. Gonza et al. (2002) used numerical simulations to examine the interaction between the impeller and volute in a centrifugal pump. They found that pressure fluctuation at blade passing frequency (f_{bpf}) had a governing effect, and its fluctuation amplitude was directly linked to the operating flow rate. Parrondo-Gayo et al. (2002) observed that the pressure fluctuation amplitude at f_{bpf} in a centrifugal pump volute was prominent at diverse flow rates. Their experimental results also highlighted the considerable influence of the interaction between the tongue and impeller on pressure fluctuations. Lin et al. (2022b) examined the relationship between pressure fluctuation and vortex fluctuation at different locations in a centrifugal pump volute. They discovered that the high-amplitude region was primarily near the volute surface and tongue, and the influence of vortex fluctuation on pressure fluctuation decreased when the flow rate increased. Lu et al. (2022) investigated the pressure fluctuation by employing the standard $k-\varepsilon$ turbulence model. They discovered a backflow vortex on the

Article Highlights

- A new method of bionic structure is proposed for the blade surface of a centrifugal pump to suppress pressure fluctuation.
- A test rig is built to measure the pressure fluctuation in pump with prototype impeller and fish scale structure impeller.
- For flow rates of 0.6 Q_d, 0.8 Q_d, 1.0 Q_d and 1.2 Q_d, the suppressions in pressure fluctuation amplitudes at fbpf are 20.98%, 5.85%, 19.20%, and 25.77%.

✉ Lei Tan
metrc@sdust.edu.cn

[1] Department of Energy and Power Engineering, Tsinghua University, Beijing 100084, China

[2] Institute of Mechanics, Chinese Academy of Sciences, Beijing 100190, China

[3] College of Mechanical and Electronic Engineering, Shandong University of Science and Technology, Qingdao 266000, China

suction surface near the tongue, which could worsen the instability of internal flow. Given the periodic impact of these vortices on the tongue, pressure fluctuations could be stimulated at the pump outlet. Oro et al. (2023) discovered that pressure fluctuation in a centrifugal pump primarily began from the interaction between the tongue and impeller, and this interaction spread along the flow path at the speed of sound. They noted that the instability of the flow in the blade channel was principally caused by the flow detachment on the pressure side when the blade operated near high flow rates. The hydrodynamic load of the blades was the leading cause of instability when the blade operated at low flow rates. Ye et al. (2024) studied the intricate relationship between pressure fluctuation and radial forces in a centrifugal pump. Their experiments revealed that blade pressure fluctuation and circumferential pressure distributions within the volute were greatly affected by operating conditions. Liu et al. (2024a) conducted numerical simulations on a multistage centrifugal pump. They discovered that the vortex structure was concentrated near the leading edge of the impeller blade, which was precisely the horseshoe vortex.

Several methods have been employed to suppress the pressure fluctuation in centrifugal pumps. Yang et al. (2023) and Liu et al. (2018) exhibited that adding guide vanes could effectively control the pressure fluctuation amplitude at f_{bpf} and f_r (rotation frequency). Zhang et al. (2015) examined how slope volutes influenced the internal flow characteristic. They designed a unique slope volute that effectively reduced interactions and inhibited pressure fluctuation amplitude. Liu et al. (2017) discovered that increasing axial distance could decrease the fluctuation amplitude at the leading edge of the vane pressure surface. Sun and Tan (2020) observed that vapor volume fraction was the basic parameter that must be considered in the design process to control the interaction between cavitation and vortex pressure fluctuations in a centrifugal pump.

Numerous bionic structures have lately been developed to improve centrifugal pump performance. Gruber et al. (2010) examined the influence of the blade trailing edge serrations. They revealed that the bionic structure could enhance the wake characteristics and suppress the vibration amplitude of most frequency bands. Gu et al. (2018) integrated the abdominal groove structure of mantis shrimp with the volute flow channel. They found that it could effectively enhance flow stability and lessen pressure fluctuation amplitude. Muthuramalingam et al. (2019; 2020) employed topological techniques to acquire the scale structure of European sea bass. They discovered that the bionic model generated stable, regular regions of low and high flow streaks on the surface. The bionic model slowed the transition from laminar to turbulent flow. Huang et al. (2021) fused the dolphin head profile with the NACA 0018 airfoil to improve the stability of the surface vortex structure and to optimize the lift coefficient and drag coefficient of the bionic airfoil. Lin et al. (2022a) fabricated a sinusoidal tubercle trailing edge by replicating the fin structure of the humpback whale, which could break the large vortex at the wake and enhance the stability of the downstream flow field. Liu et al. (2022) utilized the bionic concept in the design process of the guide vane of a centrifugal pump, which could decrease the pressure fluctuation in the clearance, vane, and casing domains. Zhao et al. (2023) applied bionic humpback whale leading-edge protuberances to pump–turbine guide vanes to expand the stable operating range of a pump–turbine. They discovered that bionic protuberances could reduce the separation vortex and reduce pressure fluctuation on the pressure surface of the vane.

The surface morphology and biological characteristics of fish have made them one of the most broadly distributed aquatic organisms and have demonstrated exceptional performance over millions of years (Zhang et al., 2021). Inspired by the excellent properties of fish scale, Yan et al. (2024) created a bionic fish scale structure on a Clark-Y hydrofoil and acquired an excellent drag-reduction effect. Afroz et al. (2016) observed that the skin shield scale of a shark could successfully manipulate the surface flow and decrease the separation of laminar and turbulent flow, as shown by experiments. Dou et al. (2012) examined the microstructure of fish scales and found that at a low-pressure state, the gas phase was formed at the solid–liquid surface owing to flow separation and eddies. These eddies decreased some of the solid–liquid shear force, thus decreasing friction drag. Muthuramalingam et al. (2019) observed different flow stripes on the surface of the fish scale with a mean velocity difference of approximately 9%. These regularly arranged stripes could impede the transition of layers to turbulent flow, resulting in a delay effect of around 55% on the Tollmien–Schlichting wave.

In summary, bionic structures demonstrate remarkable advantages in decreasing pressure fluctuation and enhancing operational stability. However, limited studies have investigated fish scale structures applied to centrifugal pump blades. This paper suggests a new design method for bionic fish scale structures on blades for a centrifugal pump. Investigations are performed to assess the effect of this bionic structure on pressure fluctuations under distinct flow rates.

2 Design method of bionic structure

Animals in nature have developed unique surface structures for survival and reproduction. Inspired by the fish scale, which possesses a perfect control ability of fluid flow on its surface, a bionic fish scale structure is established in this work. A new design method of bionic structures is offered for the blade surface in a centrifugal pump.

The geometric centers of four fish scale structural units

are arranged individually at four different vertices of a rhombus. The fish scale structural units can be set, as presented in Figure 1. These units are aligned with the fluid flow direction across the blade. The structure of a fish scale comprises a leading edge curve, a trailing edge curve, and two symmetrical side edge curves.

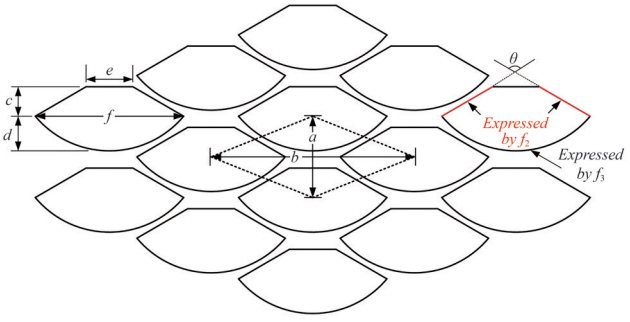

Figure 1 Bionic fish scale structure

In this work, the short diagonal of the rhombus is represented by a, the long diagonal of the rhombus is indicated by b, and $b = 5/2a$. The center of the fish scale structural unit is represented by c, and $c = 5/14a$, relative to the leading edge curve. The maximum distance from the center of the fish scale structural unit to the trailing edge curve is indicated by d, and $d = 3/7a$. The length of the leading edge curve is represented by e, and $e = 4/7a$.

The maximum distance f between the two ends of the trailing edge curve is expressed as follows:

$$f = c \cdot \tan\frac{\theta}{2} + \frac{e}{2} \tag{1}$$

The angle between the two symmetrical side edges is denoted by θ, $115° \leqslant \theta \leqslant 125°$.

The curve of the side edge can be determined as follows:

$$f_2 = -\arctan\frac{\theta}{2} \cdot \left(|x| - \frac{f}{2}\right) \tag{2}$$

The trailing edge curve can be expressed as follows:

$$f_3 = \sqrt{\left(\arctan\frac{\theta}{2} \cdot \frac{f}{2}\right)^2 - x^2} + \arctan\frac{\theta}{2} \cdot \frac{f}{2} - d \tag{3}$$

In summary, two parameters, namely a and θ, can be employed to obtain the complete fish scale structure.

Figure 2 shows the blade pressure side with the bionic fish scale structure.

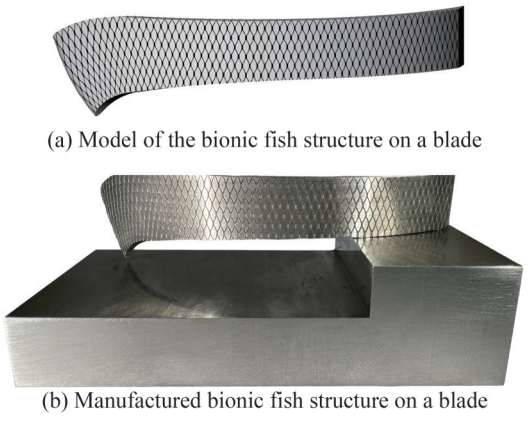

(a) Model of the bionic fish structure on a blade

(b) Manufactured bionic fish structure on a blade

Figure 2 Blade with the bionic fish scale structure

3 Experimental setup

3.1 Centrifugal pump and test rig

The prototype impeller for the centrifugal pump is developed using a method that considers the slip and diffusion effects in the impeller (Lu et al., 2024). This method aims to regard the slip effect and diffusion influence together in the impeller, and to enhance the pump performance under design and off-design conditions. The bionic impeller is fabricated by applying the fish scale structure to this prototype impeller. The fish scale structures cited in Section 2 are carved at a depth of 0.5 mm and covered on the blade surface. Laser engraving, a highly accurate surface treatment technology, is employed in manufacturing. The small heat-affected zone can inhibit material deformation during processing, and machining errors are maintained within 0.02 mm. This approach guarantees dimensional accuracy and shape consistency of the processed parts and substantially enhances the smoothness of the material surface by reducing surface roughness.

The main parameters of the centrifugal pump are enumerated in Table 1.

Table 1 Main parameters of the centrifugal pump

Parameters	Value
Rated flow rate, Q_d (m^3/h)	25
Rated head, H_d (m)	7
Rotational speed, n (rpm)	1 450
Specific speed, n_s	102
Diameter of impeller inlet, D_i (mm)	50
Diameter of impeller outlet, D_o (mm)	160
Blade number, Z	8
Rotation frequency, f_r (Hz)	24.17
Blade passing frequency, f_{bpf} (Hz)	193.33

Figure 3 illustrates the blade with a fish scale bionic structure and impeller. The closed impeller is divided into the top plate and the semi-open impeller, and five column pins are evenly distributed on the top of each blade.

The test pump is mounted in the test rig with a closed-loop pipeline system at Tsinghua University (Han and Tan,

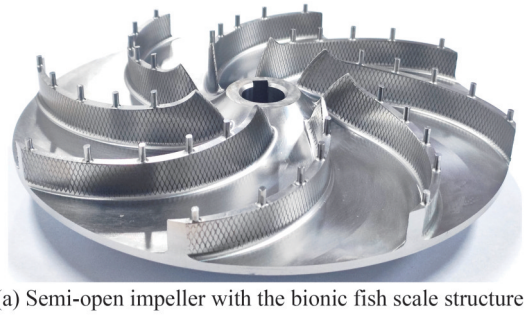

(a) Semi-open impeller with the bionic fish scale structure

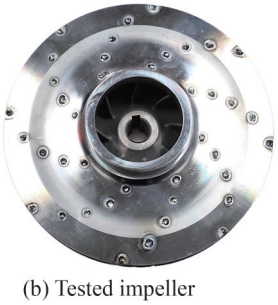

(b) Tested impeller

Figure 3 Blades and impeller with the bionic fish scale structure

2023). Figure 4 shows that the straight lengths of the inlet and outlet pipe are 17 and 19 times the diameter of the pipe, respectively, and effectively reduce the influence of cross-sectional changes on the flow stability when the fluid passes through the reducer.

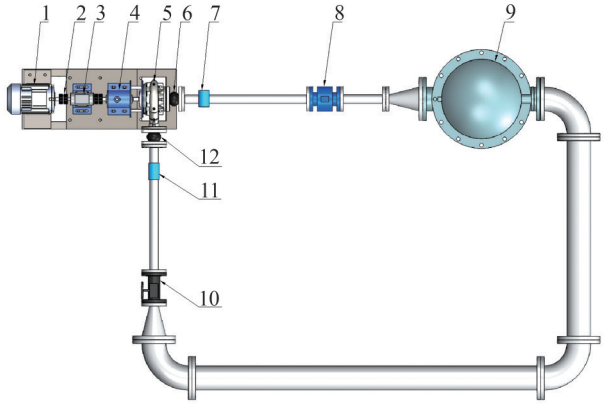

Figure 4 Scheme of the test rig for the test pump

The flow rate of the system can be controlled by modifying the opening of a globe valve. Flow rate data are gathered using an electromagnetic flowmeter with a measurement range of 0–0.083 m^3/s. The torque signals of the centrifugal pump are constantly monitored by a torque sensor with a measurement range of 0–30 N·m. Pressure transducers with a measurement range of 0–100 kPa are used to acquire pressure signals at the inlet and outlet of the centrifugal pump. The flow meter, torque meter, and pressure sensor precisions are 0.2%, 0.2%, and 0.065%, respectively.

The uncertainty E_p of transient pressure measurement is made up of the uncertainties of the standard pressure gauge, pressure transmitter, and current input isolator, which are $f_0 \leqslant \pm 0.065\%$, $f_{c_1} \leqslant \pm 0.02\%$, and $f_{c_2} \leqslant \pm 0.1\%$, respectively. Hence, E_p can be determined by employing the calculation formula for the combined standard uncertainty:

$$E_p \leqslant \sqrt{f_0^2 + f_{c_1}^2 + f_{c_2}^2} = 0.12\% \tag{4}$$

The test rig consists of: 1) motor, 2) coupling, 3) speed and torque sensor, 4) oil box, 5) test pump, 6) flexible connection, 7) pressure transducer, 8) electromagnetic flowmeter, 9) water tank, 10) valve, 11) pressure transducer, 12) flexible connection.

3.2 Signal monitor and analysis method

To measure pressure fluctuation precisely in the volute, the locations of measurement points in the volute are established by considering the actual operating conditions and volute structure. A screw thread is employed to connect the miniature pressure fluctuation sensor to the volute. The sensor's probe must be flushed with the inner wall of the flow channel to minimize its interference with the flow inside the centrifugal pump. Six measurement points are established on the circumferential surface of the volute along the flow direction, as illustrated in Figure 5.

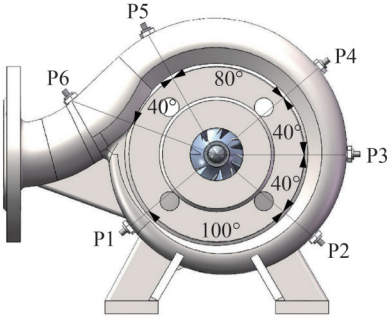

(a) Measurement points

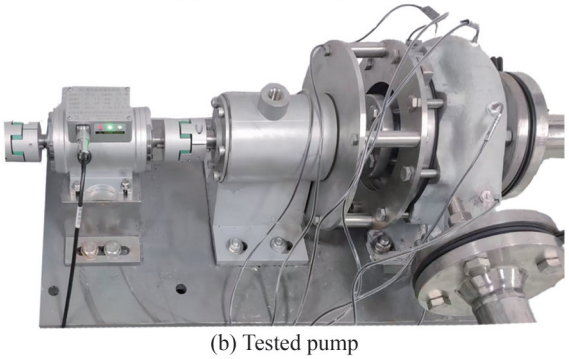

(b) Tested pump

Figure 5 Measurement points on the volute

Fourier transform is one of the frequently used methods for spectrum analysis, which can convert a time domain signal into a frequency domain signal and is employed to reflect the distribution and amplitude changes of signals at

distinct frequencies (Lu et al., 2024). The Fourier transform needs truncation due to its infinite dimension property to restrict the signal to a certain range. However, signal truncation may result in spectral leakage, which leads to an inaccurate distribution of spectral lines in the frequency domain plot. To lessen errors caused by spectral leakage, the data are generally processed by using a window function. In this work, the Hanning window is employed to smooth the original data (Ahmad et al., 2017).

The Hanning window function $\omega(t)$ is expressed as follows:

$$\omega(t)=\begin{cases}\frac{1}{2}+\frac{1}{2}\cos\left(\frac{\pi t}{T}\right), & |t|\leqslant T\\ 0, & |t|\geqslant T\end{cases} \tag{5}$$

The amplitude–frequency characteristic $W(\omega)$ of the Hanning window is expressed as follows:

$$W(\omega)=\frac{\sin(\omega T)}{\omega}\cdot\frac{1}{1-\left(\frac{\omega T}{\pi}\right)^2} \tag{6}$$

Centrifugal pumps that operate under normal conditions can be considered as having obtained continuous and periodic signals. The Fourier transform of these signals is performed in the basic form as shown below:

$$F\left[x(t)\right]=X(\omega)=\int_{-\infty}^{+\infty}x(t)\mathrm{e}^{-\mathrm{i}\omega t}\mathrm{d}t \tag{7}$$

$$\mathrm{e}^{-\mathrm{i}\omega t}=\cos(\omega t)-\mathrm{i}\sin(\omega t) \tag{8}$$

The original signal is represented by $x(t)$, the base of the natural logarithm is denoted e, and the imaginary unit is i.

In experiments, the signals used for spectral analysis are discrete data with discontinuities in the time and frequency domains. Therefore, the signals must be examined using the discrete Fourier transform:

$$X(m)=\sum_{n=0}^{N-1}x(n)\mathrm{e}^{-\mathrm{i}\frac{2\pi}{N}nm}\left(m=0,1,2,\cdots,N-1\right) \tag{9}$$

The amplitude dealt by fast Fourier transform is denoted as $X(m)$, the number of data points is represented by N, and the number of cycles is m.

4 Results and discussions

4.1 Pressure fluctuation in the time domain

Due to the intense pressure fluctuation near the tongue, the time domain signals on monitoring points near the tongue, namely, P1 and P6, are studied. The horizontal coordinate in the time–domain diagram is the time corresponding to 10 revolutions of the impeller, and the vertical coordinate signifies the pressure.

Figure 6 presents the time domain signals of pressure fluctuation at P1. Because the acquired pressure signals meet the normal distribution law, the pressure fluctuation range at the measurement point could be assessed by a confidence interval. The pressure amplitude fluctuation range is within 10.7 kPa at Q = 0.6 Q_d. As the flow rate increases, the interference improves the pressure fluctuation, so the fluctuation range of pressure amplitude at P1 gradually increases. The fluctuation range of the measurement point achieves the maximum value of 13.4 kPa at the rated flow rate. The fluctuation range of pressure amplitude decreases and stays within 9.2 kPa around Q = 1.2 Q_d.

The same test is performed by replacing the prototype impeller with the bionic impeller. Figure 7 shows that the fluctuation ranges of pressure amplitude at P1 are 10.9, 12.6, 12.7, and 8.8 kPa, while the operating flow rates are 0.6 Q_d, 0.8 Q_d, 1 Q_d, and 1.2 Q_d, respectively. Compared with the prototype impeller, the fluctuation range of pressure amplitude rises by 0.2 kPa under the 0.6 Q_d condition. By contrast, the fluctuation range declines by 0.4 kPa when the flow rate increases from 0.8 Q_d to 1.2 Q_d.

Table 2 presents that the average pressure fluctuation values at P1 of the bionic impeller are near those of the prototype impeller under the same working conditions. The average pressure fluctuation value decreases when the flow rate increases.

Figure 8 demonstrates the time domain signals of pressure fluctuation at P6. In the same time interval, the waveform and change rule at P6 is similar to that of P1 but with a larger pressure fluctuation range. The pressure fluctuation range is around 11.5 kPa when the flow rate is 0.6 Q_d. When the flow rate rises from 0.8 Q_d to 1.0 Q_d, the pressure fluctuation range expands from 14.8 kPa to 15.2 kPa. When the flow rate is further increased to 1.2 Q_d, the pressure fluctuation range narrows to 11.0 kPa because the interaction between the tongue and impeller causes the pressure fluctuation, which is one of the principal sources of fluctuating energy. When the pressure fluctuation is transmitted to the vicinity of P6, the obstruction of the tongue leads to some attenuation of the fluctuating energy, which diminishes the range of pressure fluctuation.

Figure 9 shows the pressure fluctuation at P6 of the bionic impeller, and its amplitude fluctuation range decreases at low flow rates. The pressure amplitude fluctuation range increases at design and high flow rate conditions. The pressure amplitude fluctuation ranges at P6 are 11.3, 14.4, 16.5, and 11.7 kPa, while the operating flow rates are 0.6 Q_d, 0.3 Q_d, 1.0 Q_d, and 1.2 Q_d, respectively. Compared with the prototype impeller, the fluctuation range of the bionic impeller under low flow rates decreases by 0.2 kPa and

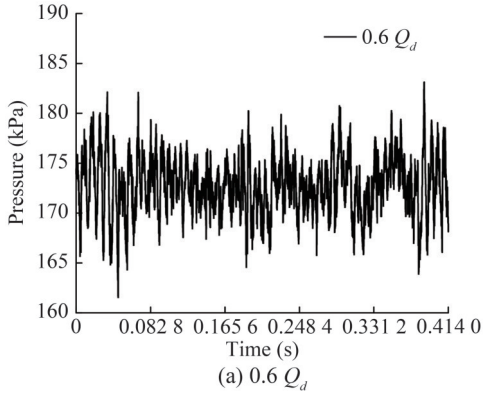

Figure 6 Pressure fluctuation at P1 of prototype impeller

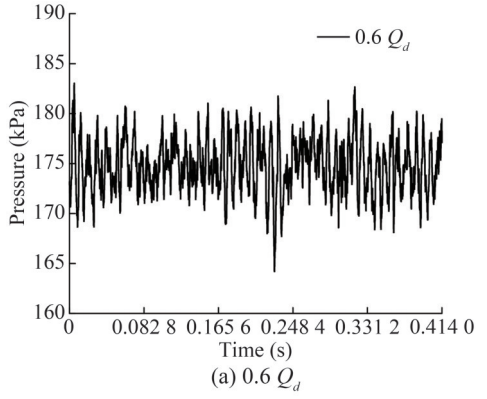

Figure 7 Pressure fluctuation at P1 of bionic impeller

0.4 kPa, respectively. By contrast, the fluctuation range increases by 1.3 kPa and 0.7 kPa under design and high flow rates, respectively.

Table 3 shows that compared with P1, the average pressure fluctuation value at P6 is higher at the low flow rates but lower at the rated condition and high flow rates.

Table 2 Average pressure fluctuation at P1 of prototype and bionic impellers

Flow rate	Value (kPa)	
	Prototype impeller	Bionic impeller
0.6 Q_d	173.8	173.6
0.8 Q_d	168.7	169.1
1.0 Q_d	163.6	163.8
1.2 Q_d	158.3	158.1

In this section, time–domain analysis is employed to illustrate intuitively the change of the signal over time and the influence of the bionic structure on pressure pulsation. The following section will discuss an in-depth investigation of frequency components and energy distribution of the pressure pulsation signal.

4.2 Pressure fluctuation in the frequency domain

Centrifugal pumps display characteristic frequencies relating to the f_r and f_{bpf} and their harmonic frequency. The frequency domain signals of pressure fluctuation at the circumferential measurement points of the volute gathered in the experiment are concentrated in the region within 3–4 times the f_{bpf}. Hence, the spectral characteristic analysis only includes the range of 0–5 times f_{bpf}. The horizontal axis of the frequency domain plots is normalized to facilitate an intuitive examination of pressure fluctuations in the volute channel. The primary scale of the plot represents f_{bpf} and its harmonic frequency, whereas the secondary scale denotes the f_r and its harmonic frequency.

In the investigation of the variation of pressure fluctuation produced by unsteady flow at different flow rates, the pressure signal is dimensionless, and the intensity of the fluctuation is denoted by the pressure coefficient C_p as follows:

$$C_P = \frac{P - \overline{P}}{0.5\rho {u_2}^2} \tag{10}$$

In Equation (9), P is the instantaneous pressure, $\overline{P}$ is the average pressure, and u_2 is the circumferential velocity at the outlet.

Figures 10–13 present the pressure fluctuations at monitoring points under four unique flow rates of the measured pump. The frequency of pressure fluctuation is dominated by f_r, f_{bpf}, and their harmonic frequency. The pressure fluctuations at the frequency of f_{bpf} are triggered by the periodic traversal of the volute by the impeller blades during rotation (Jia et al., 2024). Owing to the structure of the tongue, numerous complex flows are around its vicinity. The vigorous interaction in this area strengthens pressure fluctuations near the tongue (Yang et al., 2022). The monitoring points nearer to the tongue demonstrate an increased global pressure fluctuation amplitude, and the main frequency is f_{bpf}. Monitoring points farther from the tongue show lower amplitude pressure fluctuations, dominated by chaos smaller than f_{bpf} (Canepa et al., 2016).

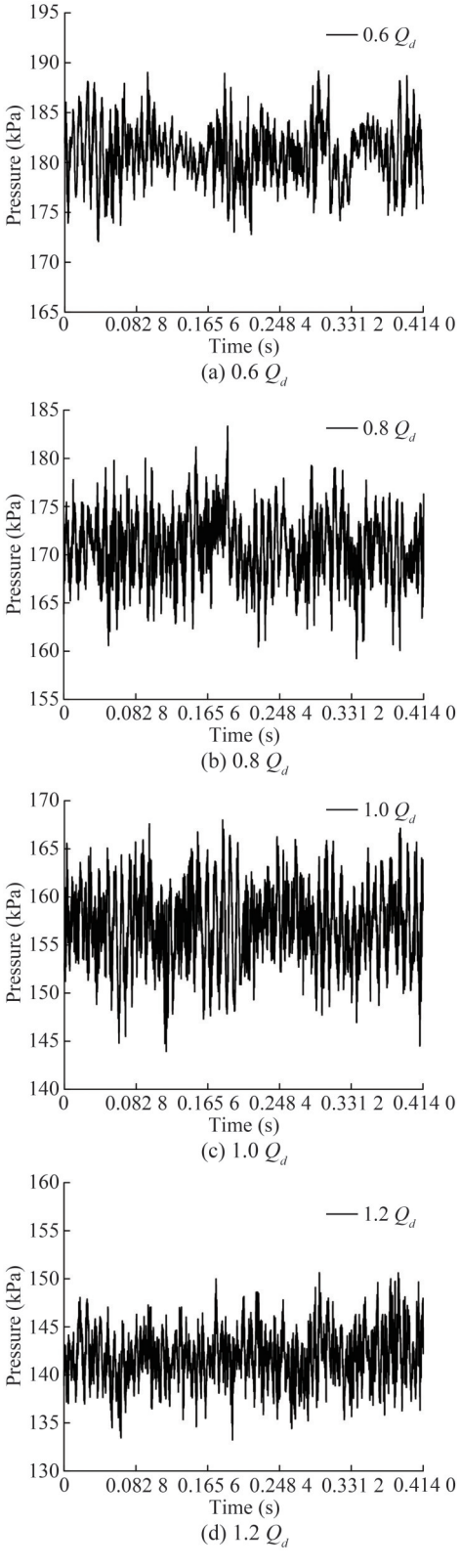

Figure 8 Pressure fluctuation at P6 of prototype impeller

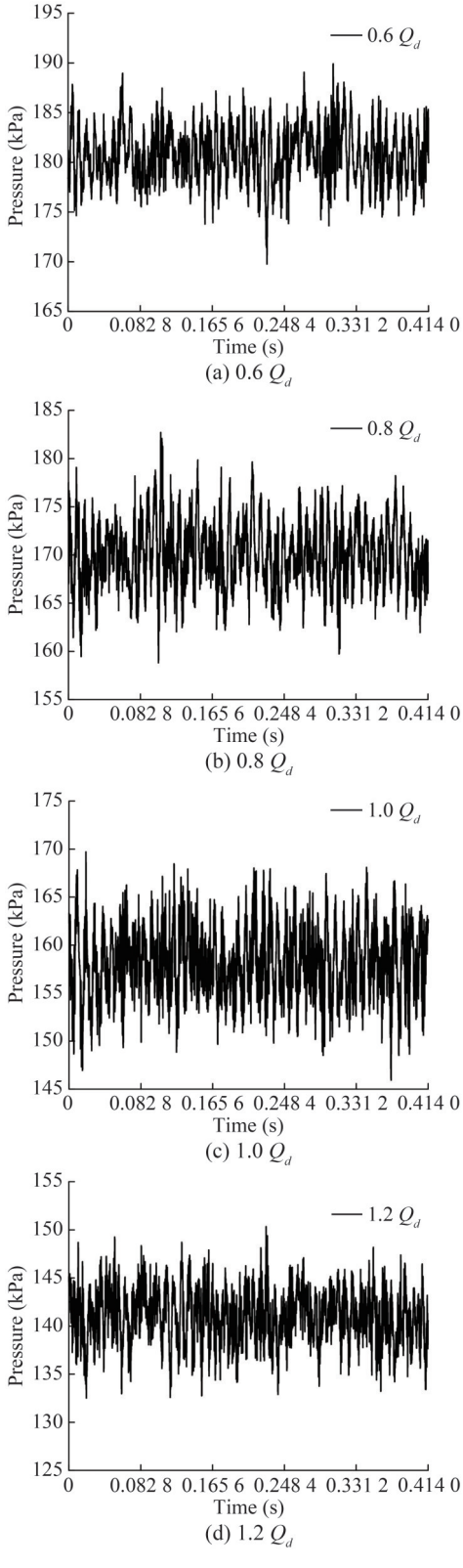

Figure 9 Pressure fluctuation at P6 of bionic impeller

Pressure fluctuation in the circumferential flow channel decreases and then increases along the spiral line in the volute. The pressure fluctuation in the volute flow path is substantially affected by the interaction between the impeller and tongue (Al-Obaidi, 2019). P1, at the beginning of the spiral line, has a high amplitude of pressure fluctuations at f_{bpf}. Because P3 is the farthest from the tongue, its pressure fluctuation decreases in amplitude. As the flow toward the outlet, the influence of the interaction gradually increases. The interaction between the impeller and tongue is the source of a peak in pressure fluctuation at point P6 again. Complex fluctuation amplitudes in the frequency domain at the low-frequency region from 0 to f_{bpf} are produced by the influence of the secondary flow, flow separation, vortex in the pump, and other complex flows interfering with one another (Li et al., 2016). Moreover, the experimental system is characterized by inherent uncertainty due to manufacturing and installation errors (Kim et al., 2023).

Table 3 Average pressure fluctuation at P6 of prototype and bionic impellers

Flow rate	Value (kPa)	
	Prototype impeller	Bionic impeller
0.6 Q_d	180.9	180.7
0.8 Q_d	170.5	170.1
1.0 Q_d	157.2	157.9
1.2 Q_d	141.9	141.2

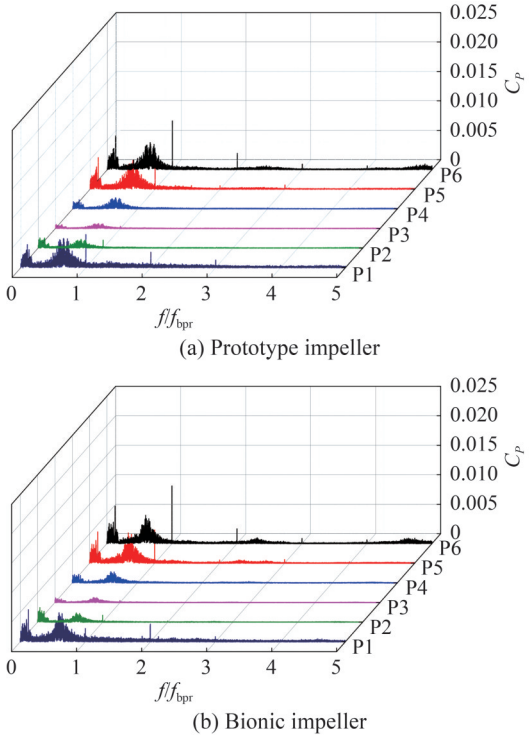

Figure 10 Pressure fluctuation distribution in the volute under 0.6 Q_d

Figure 10 presents the pressure fluctuations in the volute under 0.6 Q_d. The amplitude of pressure fluctuations in the volute is low at the 0.6 Q_d condition. f_r signal is captured at most monitoring points, with the dominant frequency of

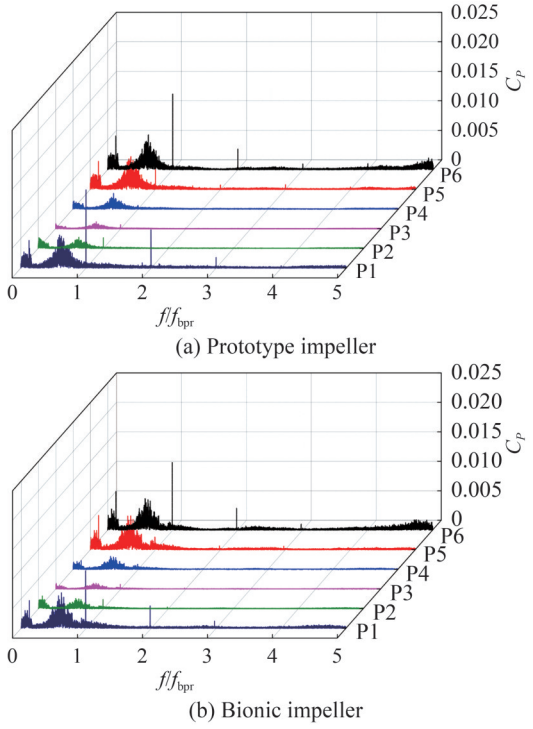

Figure 11 Pressure fluctuation distribution in the volute under 0.8 Q_d

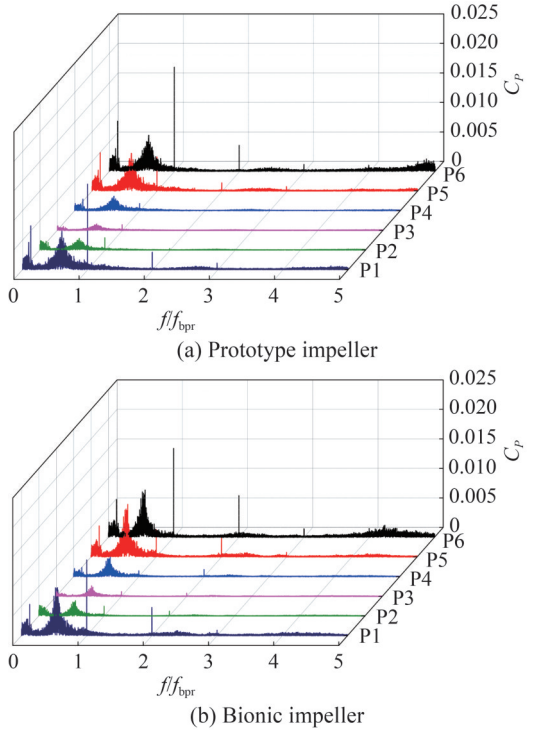

Figure 12 Pressure fluctuation distribution in the volute under 1.0 Q_d

f_{bpf} at P1 and P6, whereas the fluctuation amplitude at the other measurement points is mostly low. The pressure fluctuation distribution of the bionic impeller is revealed in Figure 10(b). The amplitude of P1 at f_{bpf} decreases, and the main frequency changes to f_r. The main frequency amplitude of P6 rises slightly, and the fluctuation intensity improves.

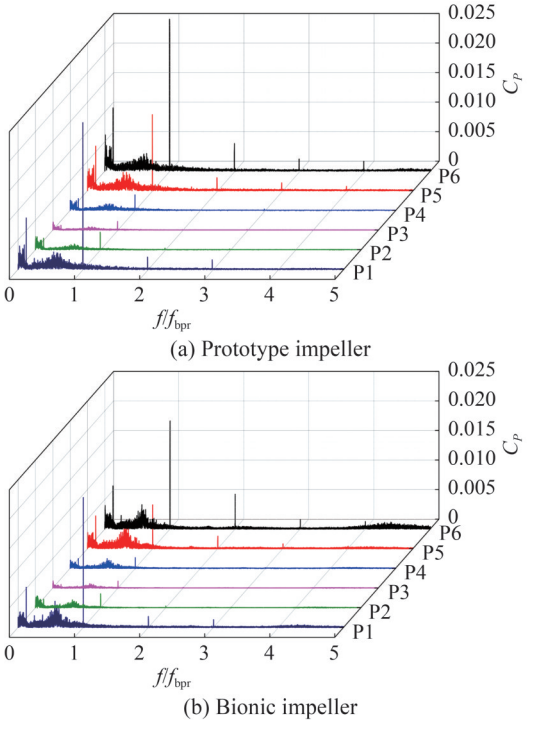

Figure 13 Pressure fluctuation distribution in the volute under 1.2 Q_d

By contrast, the monitoring points farther from the tongue are less influenced by these changes.

The frequency amplitude rises when the flow rate increases to 0.8 Q_d. Figure 11 presents that the bionic structure can considerably diminish the amplitudes at f_{bpf} and its second harmonic frequency around P1 and P6. This outcome is primarily because the bionic structure modifies flow states in the near-wall area when fluid flows through the blade, increases energy consumption, and decreases pressure pulsation amplitude (Chen et al., 2024).

Figure 12 presents the pressure fluctuations in the volute under 1.0 Q_d. The amplitudes in the broadband frequency region and at f_{bpf} increase compared to that at 0.8 Q_d. The amplitude at f_{bpf} is suppressed when the bionic impeller is employed.

Figure 13 reveals the pressure fluctuations in the volute under 1.2 Q_d. The amplitudes at f_{bpf} and broadband frequency increase with the increasing flow rate. The bionic impeller could lower the amplitude at f_{bpf}. Under high flow rate conditions, the pressure fluctuation amplitudes at f_r and f_{bpf} achieve the highest values. A higher amplitude of broadband pressure fluctuation is observed in the bionic impeller than in the prototype impeller. This phenomenon is ascribed to the bionic structure influencing the near-wall region flow near the blade surface, which disperses fluid energy and strengthens the mutual interference between the complex flows (Dou, 2012).

4.3 Comparison of main frequency amplitudes

The primary frequency amplitudes at each measurement

point on the centrifugal pump increase as the flow rate increases. This outcome is largely ascribed to the interaction between the rotating impeller and the static tongue, which comprises the primary source of pressure fluctuation. The increased flow rate leads to a higher fluid velocity within the pump and a corresponding increment of the impact force on the volute. A stronger wall shear stress is produced, which further intensifies interactions and increases its fluctuation amplitude (Liu et al., 2024b).

The interaction between the impeller and tongue leads to the main fluctuation frequency at f_{bpf}. Table 4 presents the fluctuation amplitudes at f_{bpf} under diverse measurement points and flow rates. With the increase of flow rate, the fluctuation amplitudes at f_{bpf} steadily increase in the volute. The monitoring points nearer to the tongue have higher fluctuation amplitudes at f_{bpf}. This outcome proves that the interaction between the impeller and tongue is the principal factor in the centrifugal pump. When the bionic impeller is employed, discernible reductions in the amplitudes at f_{bpf} are collected at all monitoring points on the centrifugal pump. The decrease is specifically noticeable nearer to the tongue. Lin et al. (2024) determined that bionic structures could suppress the formation of large-scale vortices in the impeller by modifying the blade channel structure, which lessens the effect of vortex evolution on local pressure fluctuations. Bionic structures can change the flow layout on the blade surface, which can essentially prevent flow separation and the generation of large vortices according to Wei et al. (2024). From flow rates of 0.6 Q_d to 1.2 Q_d, average suppressions in pressure fluctuation amplitudes at f_{bpf} are 20.98%, 5.85%, 19.20%, and 25.77%.

Figure 14 exhibits the pressure fluctuation amplitude at f_{bpf} with diverse flow rates. The highest amplitude of the prototype impeller at f_{bpf} under the conditions of 0.8 Q_d and 1.2 Q_d is at P1. The highest amplitude at f_{bpf} under the conditions of 0.6 Q_d and 1.0 Q_d in the prototype impeller is P6. In the bionic impeller, the highest amplitude at f_{bpf} under the conditions of 0.6 Q_d, 0.8 Q_d, and 1.0 Q_d is at P6, whereas the highest amplitude at f_{bpf} under the conditions of 1.2 Q_d is at P1.

Table 4 Pressure fluctuation amplitude (C_p) at f_{bpf}

Flow rate	Impeller	P1	P2	P3	P4	P5	P6
0.6 Q_d	Prototype	0.005 6	0.001 3	0.000 4	0.000 3	0.005 7	0.008 3
	Bionic	0.002 3	0.001 2	0.000 3	0.000 1	0.005 6	0.009 8
0.8 Q_d	Prototype	0.013 2	0.001 8	0.000 7	0.000 6	0.003 5	0.012 8
	Bionic	0.009 8	0.001 5	0.000 8	0.000 9	0.002 2	0.011 5
1.0 Q_d	Prototype	0.014 5	0.002 1	0.000 9	0.001 2	0.005 8	0.017 6
	Bionic	0.012 8	0.001 6	0.000 8	0.001 0	0.004 6	0.015 1
1.2 Q_d	Prototype	0.024 9	0.003 0	0.001 5	0.002 6	0.012 9	0.025 7
	Bionic	0.022 0	0.002 4	0.001 2	0.001 8	0.007 4	0.018 3

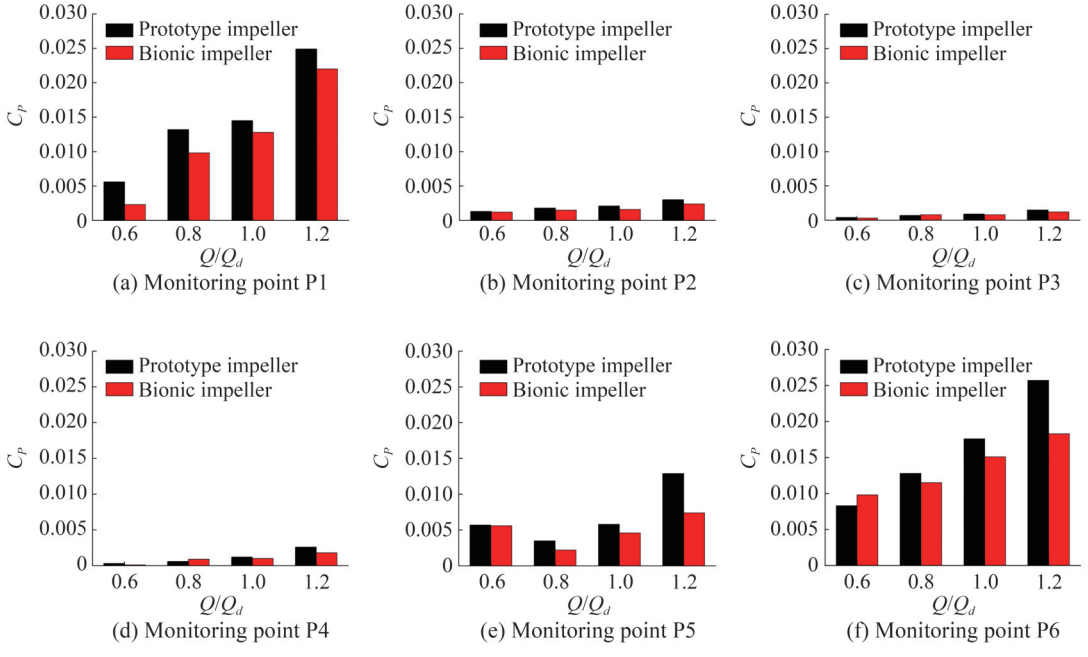

Figure 14 Pressure fluctuation amplitude at f_{bpf} for prototype impeller and bionic impeller

When the bionic impeller is employed, the decreases in amplitude at f_{bpf} at P1 are 60.71%, 26.52%, 12.50%, and 11.29% from flow rates of 0.6 Q_d to 1.2 Q_d. At P6, the opposite trend is observed, and the suppression effect on the amplitude at f_{bpf} is gradually strengthened. When flow rates rise from 0.8 to 1.2 Q_d, the amplitude at f_{bpf} at P6 declines by 9.52%, 14.77%, and 19.74%.

5 Conclusions

This work presents an innovative bionic blade surface design method for a single-stage centrifugal pump inspired by fish scale structures. An experimental system is built to investigate the pressure fluctuation characteristics in the pump. The primary conclusions drawn are enumerated below:

1) A new method of bionic structure is proposed for the blade surface of a centrifugal pump. The fish scale structure comprises a leading edge, a trailing edge, and two symmetrical side edges.

2) Based on the arrangement characteristics of fish scale structures on the fish body surface that inhibit pressure fluctuation, the fish scale structure is covered on the blade surface, and a test rig for the centrifugal pump is developed to assess the pressure fluctuation in pump with prototype impeller and fish scale structure impeller.

3) Experimental measurements reveal that the fish scale structure can remarkably inhibit the pressure fluctuation in the centrifugal pump. From a flow rate of 0.6 Q_d to 1.2 Q_d, the average suppressions in pressure fluctuation amplitudes at f_{bpf} are 20.98%, 5.85%, 19.20%, and 25.77%.

The proposed fish scale structure in this work can effectively suppress pressure pulsations in a centrifugal pump, and future work can optimize the geometry of the proposed fish scale or novel fish scale.

Funding This work has been supported by the Open Fund of Science and Technology on Thermal Energy and Power Laboratory [TPL2021A02], the State Key Laboratory of Hydroscience and Engineering [sklhse-2023-E-01].

Competing interest The authors have no competing interests to declare that are relevant to the content of this article.

References

Al-Obaidi AR (2019) Investigation of effect of pump rotational speed on performance and detection of cavitation within a centrifugal pump using vibration analysis. Heliyon 5(6). https://doi.org/10.1016/j.heliyon.2019.e01910

Ahmad M, Jung LT, Bhuiyan AA (2017) From DNA to protein: Why genetic code context of nucleotides for DNA signal processing? A review. Biomedical Signal Processing and Control 34: 44-63. https://doi.org/10.1016/j.bspc.2017.01.004

Afroz F, Lang A, Habegger ML, Motta P, Hueter R (2016) Experimental study of laminar and turbulent boundary layer separation control of shark skin. Bioinspiration and biomimetics 12(1): 016009. https://doi.org/10.1088/1748-3190/12/1/016009

Canepa E, Cattanei A, Zecchin FM, Milanese G, Parodi D (2016) An experimental investigation on the tip leakage noise in axial-flow fans with rotating shroud. Journal of Sound and Vibration 375: 115-131. https://doi.org/10.1016/j.jsv.2016.04.009

Chen H, Zhang T, Han Z, Huang H, Chen H, Gao Q (2024) Battery thermal management enhancement based on bionics. International Communications in Heat and Mass Transfer 157: 107756. https://doi.org/10.1016/j.icheatmasstransfer.2024.107756

Dou Z, Wang J, Chen D (2012) Bionic research on fish scales for drag reduction. Journal of Bionic Engineering 9(4): 457-464. https://doi.org/10.1016/s1672-6529(11)60140-6

Duplaa S, Coutier-Delgosha O, Dazin A, Roussette O, Bois G, and Caignaert G (2010) Experimental study of a cavitating centrifugal pump during fast startups. Journal of Fluid Engineering 132(2): 021301. https://doi.org/10.1115/1.4000845

Fu Q, Zhang F, Zhu R, He B (2016) A systematic investigation on flow characteristics of impeller passage in a nuclear centrifugal pump under cavitation state. Annals of Nuclear Energy 97: 190-197. https://doi.org/10.1016/j.anucene.2016.07.011

Gonzá lez J, Ferná ndez JN, Blanco E, Santolaria C (2002) Numerical simulation of the dynamic effects due to impeller-volute interaction in a centrifugal pump. J. Fluids Eng 124(2): 348-355. https://doi.org/10.1115/1.1457452

Gruber M, Joseph P, Chong TP (2010, November) Experimental investigation of airfoil self noise and turbulent wake reduction by the use of trailing edge serrations. In 16th AIAA/CEAS aeroacoustics conference (p. 3803). https://doi.org/10.2514/6.2010-3803

Gu Y, Zhang W, Mou J, Zheng S, Zhou P, Fan T (2018) Effect of bionic mantis shrimp groove volute on vortex pump pressure pulsation. Journal of Central South University 25(10): 2399-2409. https://doi.org/10.1007/s11771-018-3924-3

Huang S, Hu Y, Wang Y (2021) Research on aerodynamic performance of a novel dolphin head-shaped bionic airfoil. Energy 214: 118179. https://doi.org/10.1016/j.energy.2020.118179

Han Y, Tan L (2023) Experimental investigation on spatial-temporal evolution of tip leakage cavitation in a mixed flow pump with tip clearance. International Journal of Multiphase Flow 164: 104445. https://doi.org/10.1016/j.ijmultiphaseflow. 2023.104445

Jia Z, Zhang S, Fang K, Kong B, Xie M, Zhang Q, Yang C (2024) Assessment of stress-blended eddy simulation on prediction of flow characteristics in a Rushton impeller stirred tank. Chemical Engineering Science 284: 119442. https://doi.org/10.1016/j.ces.2023.119442

Kim S, Pak M, Kim YJ, Lee H (2023) Motor noise source identification and tub vibration prediction in a drum washing machine. Applied Acoustics 210: 109434. https://doi.org/10.1016/j.apacoust.2023.109434

Li C, Lin Q, Ding X, Ye X (2016) Performance, aeroacoustics and feature extraction of an axial flow fan with abnormal blade angle. Energy 103: 322-339. https://doi.org/10.1016/j.energy.2016.02.147

Lin T, Zhang J, Li J, Li X, Zhu Z (2022b) Pressure fluctuation–vorticity interaction in the volute of centrifugal pump as hydraulic turbines (PATs). Processes 10(11): 2241. https://doi.org/10.3390/pr10112241

Lin T, Zhang J, Wei B, Zhu Z, Li X (2024) The role of bionic tubercle leading-edge in a centrifugal pump as turbines (PATs). Renewable Energy 222: 119869. https://doi.org/10.1016/j.renene.

2023.119869
Lin Y, Li X, Zhu Z, Wang X, Lin T, Cao H (2022a) An energy consumption improvement method for centrifugal pump based on bionic optimization of blade trailing edge. Energy 246: 123323. https://doi.org/10.1016/j.energy.2022.123323
Liu B, Zhang W, Chen F, Cai J, Wang X, Liu Y, Zhang J, Wang Q (2024a) Performance prediction and optimization strategy for LNG multistage centrifugal pump based on PSO-LSSVR surrogate model. Cryogenics 140: 103856. https://doi.org/10.1016/j.cryogenics.2024.103856
Liu H, Wang X, Lu Y, Yan Y, Zhao W, Wu X, Zhang Z (2022) Application and optimal design of the bionic guide vane to improve the safety serve performances of the reactor coolant pump. Nuclear Engineering and Technology 54(7): 2491-2509. https://doi.org/10.1016/j.net.2022.01.031
Liu J, Zhang F, Song M, Zhu L, Appiah D, Yuan S (2024b) Effects of unstable flow structures on energy transfer mechanism in a centrifugal pump. Proceedings of the Institution of Mechanical Engineers, Part A: Journal of Power and Energy 238(1): 73-89. https://doi.org/10.1177/09576509231195222
Liu M, Tan L, Cao S (2018). Influence of geometry of inlet guide vanes on pressure fluctuations of a centrifugal pump. Journal of Fluids Engineering 140(9): 091204. https://doi.org/10.1115/1.4039714
Liu Y, Tan L, Liu M, Hao Y, Xu Y (2017) Influence of prewhirl angle and axial distance on energy performance and pressure fluctuation for a centrifugal pump with inlet guide vanes. Energies 10(5): 695. https://doi.org/10.3390/en10050695
Lu J, Chen Q, Liu X, Zhu B, Yuan S (2022) Investigation on pressure fluctuations induced by flow instabilities in a centrifugal pump. Ocean Engineering 258: 111805. https://doi.org/10.1016/j.oceaneng.2022.111805
Lu Y, Tan L (2024) Design method based on a new slip-diffusion parameter of centrifugal pump for multiple conditions in wide operation region. Energy 294: 130796. https://doi.org/10.1016/j.energy.2024.130796
Lu Y, Tan L, Zhao X, Ma C (2024) Experiment on cavitation-vibration correlation of a centrifugal pump under steady state and start-up conditions in energy storage station. Journal of Energy Storage 83: 110763. https://doi.org/10.1016/j.est.2024.110763
Majidi K (2005) Numerical study of unsteady flow in a centrifugal pump. J. Turbomach 127(2): 363-371. https://doi.org/10.1115/1.1776587
Muthuramalingam M, Puckert DK, Rist U, Bruecker C (2020) Transition delay using biomimetic fish scale arrays. Scientific Reports 10(1): 14534. https://doi.org/10.1038/s41598-020-71434-8
Muthuramalingam M, Villemin LS, Bruecker C (2019) Streak formation in flow over biomimetic fish scale arrays. Journal of Experimental Biology 222(16): jeb205963. https://doi.org/10.1242/jeb.205963
Oro JF, Perotti RB, Vega MG, González J (2023) Effect of the radial gap size on the deterministic flow in a centrifugal pump due to impeller-tongue interactions. Energy 278: 127820. https://doi.org/10.1016/j.energy.2023.127820
Parrondo-Gayo JL, Gonzá lez-Pé rez J, Ferná ndez-Francos JN (2002) The effect of the operating point on the pressure fluctuations at the blade passage frequency in the volute of a centrifugal pump. J. Fluids Eng 124(3): 784-790. https://doi.org/10.1115/1.1493814
Sun W, Tan L (2020) Cavitation-vortex-pressure fluctuation interaction in a centrifugal pump using bubble rotation modified cavitation model under partial load. Journal of Fluids Engineering 142(5): 051206. https://doi.org/10.1115/1.4045615
Van Rhyn P, Pretorius JHC (2018) Increasing Water Pump Station Throughput by Introducing VFD-Based IE4 Class Synchronous Reluctance Motors with Improved Pump Control. In 2018 IEEE International Conference on Environment and Electrical Engineering and 2018 IEEE Industrial and Commercial Power Systems Europe (EEEIC/I&CPS Europe) (pp. 1-6). IEEE. https://doi.org/10.1109/EEEIC.2018.8494393
Wei X, Li D, Li S, Chang H, Fu X, Zuo Z, Wang H (2024) Effect of leading-edge protuberances on swept wing aircraft performance. International Journal of Fluid Engineering 1(3): 033101. https://doi.org/10.1063/5.0203063
Yin J, Song Y, Huang G, Cai K, Wang D (2020) Experimental validation of an innovative design of bubble column reactor. International Journal of Heat and Mass Transfer 156: 119597. https://doi.org/10.1016/j.ijheatmasstransfer.2020.119597
Yang G, Shen X, Shi L, Meng J, Luo W, Zhang D, van Esch BB (2023) Unsteady numerical investigations of the effect of guide vane openings on the hydrodynamic characteristics under stall conditions in a pump-turbine pump mode. Energy Conversion and Management 293: 117499. https://doi.org/10.1016/j.enconman.2023.117499
Yang M, Shu M, Wang X, Deng K, Yang B, Martinez-Botas R (2022) Rotor-stator aerodynamic interaction of centrifugal compressor at pulsating backpressure conditions. International Journal of Heat and Fluid Flow 96: 109009. https://doi.org/10.1016/j.ijheatfluidflow.2022.109009
Yan H, Xie T, Wang F, Zeng Y, Ai J (2024) Effect of biomimetic fish scale structure on the drag reduction performance of Clark-Y hydrofoil. Proceedings of the Institution of Mechanical Engineers Part M: Journal of Engineering for the Maritime Environment, 14750902241228153. https://doi.org/10.1177/14750902241228153
Ye C, Xia K, Yan H, Cao S, Wang Z, Tian Q, van Esch B, Zheng Y, Yang C (2024) Study on the influence of volute structure on the performance of seawater-pumped storage hydropower plant unit. Journal of Energy Storage 90: 111848. https://doi.org/10.1016/j.est.2024.111848
Zhao Y, Li D, Chang H, Fu X, Wang H, Qin D (2023) Suppression effect of bionic guide vanes with different parameters on the hump characteristics of pump-turbines based on entropy production theory. Energy 283: 128650. https://doi.org/10.1016/j.energy.2023.128650
Zhang K, Ma C, Zhang J, Zhang B, Zhao B (2021) Drag reduction characteristics of bionic structure composed of grooves and mucous membrane acting on turbulent boundary layer. Journal of Applied Fluid Mechanics 15(1): 283-292. https://doi.org/10.47176/jafm.15.01.32901
Zhang N, Yang M, Gao B, Li Z, Ni D (2015) Experimental investigation on unsteady pressure pulsation in a centrifugal pump with special slope volute. Journal of Fluids Engineering 137(6): 061103. https://doi.org/10.1115/1.4029574